53rd IEEE Conference on Decision and Control
December 15-17, 2014. Los Angeles, California, USA

State Estimation of Vehicle's Lateral Dynamics using Unscented Kalman Filter

Mark Wielitzka[1], Matthias Dagen[2], and Tobias Ortmaier[3]

Abstract— **In order to improve vehicle's active safety systems accurate knowledge about the vehicle's driving stability is necessary. Especially the exact determination of the side-slip angle can be of great importance, since it has major potential for improving current control algorithms. Therefore, a model-based methodology for online estimation of vehicle's lateral dynamics is presented, while generalizations of the Kalman Filter algorithm, the Extended and Unscented Kalman Filters are used due to the highly non-linear model behavior.**

The results of the introduced methodologies are presented for two different driving maneuvers and validated comparing to measurements taken with a VW Golf GTI. Furthermore, a qualitative comparison between Extended and Unscented Kalman Filter is realized.

I. INTRODUCTION

Vehicle stability control systems that increase the vehicle's active safety have gained interest in the past few decades. Systems that prevent from spinning, drifting, or rolling over have been developed and implemented in modern cars by several automotive manufacturers. However, there is still a major potential in improving these systems by using additional control parameters. Due to physical and economic reasons some of the interesting states describing vehicle's lateral dynamics, e.g. the vehicle's side-slip angle, cannot be measured directly. Therefore, an accurate and robust methodology for online estimation of the side-slip angle needs to be developed. In this context two different approaches are present in current research activities. First, Global Positioning System (GPS) based methods using a combination of inertial measurements and GPS data [1]. These systems lack of reliability in absence of GPS data, e.g. while passing a tunnel. Additionally, the low rate of measurement data of 10 - 20 Hz [2] is ineffective for online implementation of these systems. Therefore, the second approach relying on model based methodologies using a combination of inertial measurements taken by serial sensors implemented in current vehicles and a parametric physical model describing the vehicle's dynamics has been proposed. We will focus on the second approach due to the mentioned disadvantages of the first method. Obviously, the estimators' performance and, therefore, their commercial success is strongly dependent on the used algorithms and the accuracy of the underlying parametric model. Thus, a tradeoff between a detailed model and complex estimation algorithms on one hand and computational effort on the other has to be found.

To reduce this computational effort, many publications concerning vehicle's state estimation use highly simplified dynamic models. For example considering the bicycle model [3], [4] or a planar two-track model (Fig. 1) [5] with linearized model equations or using an empiric model for the tire-road contact [6]. Since these simplifications lead to severe errors in estimation accuracy, in some publications more detailed models are used [7] regarding more degrees of freedom, e.g. pitch angle and more detailed representation of various influences, e.g. wheel loads and self-aligning torques. This is accompanied by a larger number of parameters and higher computational effort.

Moreover, different approaches in state estimation algorithms are considered in current research. In context with most publications in the field of vehicle dynamics the Extended Kalman Filter (EKF) [8] is used with a limited number of states [7], [9], [10] or with an enlarged state representation [11]. Using the EKF approximate noise representations for model and measurement strongly influence the estimation at every time step. Hence, a reasonable setting of these parameters has to be found, covering a variety of possible maneuvers. But since the model's behavior is strongly non-linear and corrupted not only by additive noise, a more accurate generalization, the Unscented Kalman Filter

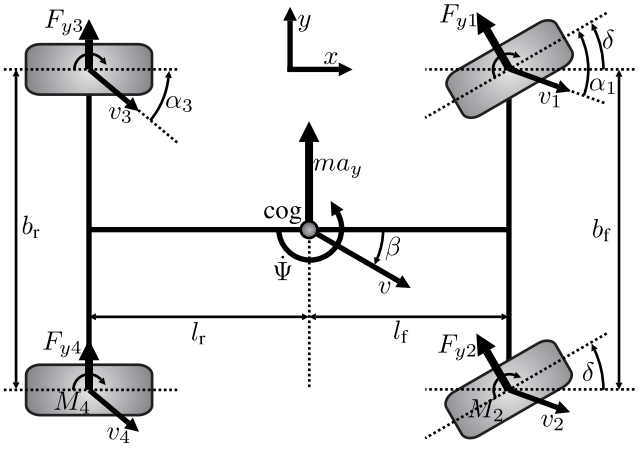

Fig. 1. Two-track model of a vehicle performing a left turn. Displayed are the geometrical parameters $l_{f,r}$, $b_{f,r}$, skew angles $\alpha_{1,3}$, lateral forces F_{yi}, self-aligning torques $M_{2,4}$, steering input δ and the resulting states β and $\dot{\Psi}$. The resulting lateral acceleration acts on the center of gravity (cog).

[1]Mark Wielitzka, Research Assistent, Institute of Mechatronic Systems, Leibniz University Hannover, 30167 Hanover, Germany mark.wielitzka@imes.uni-hannover.de

[2]Matthias Dagen, Senior Research Engineer, Institute of Mechatronic Systems, Leibniz University Hannover, 30167 Hanover, Germany matthias.dagen@imes.uni-hannover.de

[3]Tobias Ortmaier, Institute Director, Institute of Mechatronic Systems, Leibniz University Hannover, 30167 Hanover, Germany tobias.ortmaier@imes.uni-hannover.de

(UKF) [12] is employed. Using this algorithm no restrictions w.r.t noise terms have to be made by applying augmented state variables. Thereby, the mean and covariance of a random variable can be estimated up to the third order moment for any non-linearity. This approach and several further developments are used in many fields of modern engineering (e.g. [13], [14]). In special cases of Gaussian additive noise the UKF has already been used for side-slip estimation [15], [16], but again, with a limited number of states. Since current estimations still not reach the needed accuracy and robustness further improvements have to be developed.

In this paper an implementation using the general Unscented Kalman Filter algorithm, including augmented state variables is presented, while applying a detailed two-track model including roll dynamics, with an enlarged state representation. Thus, considering a static and a dynamic maneuver, the UKF's superiority over the EKF can be shown. Adjusting one setting for the UKF and EKF, respectively, the accuracy of the UKF's estimation overcomes the EKF's, considering both maneuvers.

The paper is organized as follows, in section II a two-track model with three degrees of freedom is introduced. Furthermore, the non-linear relation between skew angles and wheel loads and the tire's lateral force, respectively is implemented by parametric nonlinear functions. In section III the Kalman Filter and its generalizations the Extended and Unscented Kalman Filter are introduced and their implementation in vehicle dynamics estimation is described. The validation of the developed methodology is demonstrated in section IV by comparing state estimation and reference measurements of two different driving maneuvers.

II. Vehicle Dynamics Model

In this section a detailed parametric model for calculating vehicle's lateral dynamics including the roll angle's influence on the tire's skew angle is presented [17], [18], [19]. Since this model will be implemented in an online estimator, a trade-off between accuracy and computational effort has to be found.

A. Two-Track Model

Considering a two-track model with three degrees of freedom as displayed in Fig. 1 and 2 the lateral dynamics under disregard of vertical and longitudinal dynamics can be described by the vehicle's side-slip angle β, its yaw-rate $\dot{\Psi}$ and the roll angle κ. These quantities represent the angle between the vehicle's longitudinal axis and its velocity vector, the angular velocity of rotation around the vertical axis, and the angle between the vehicle's vertical axis and the stationary vertical axis, respectively. This leads to the

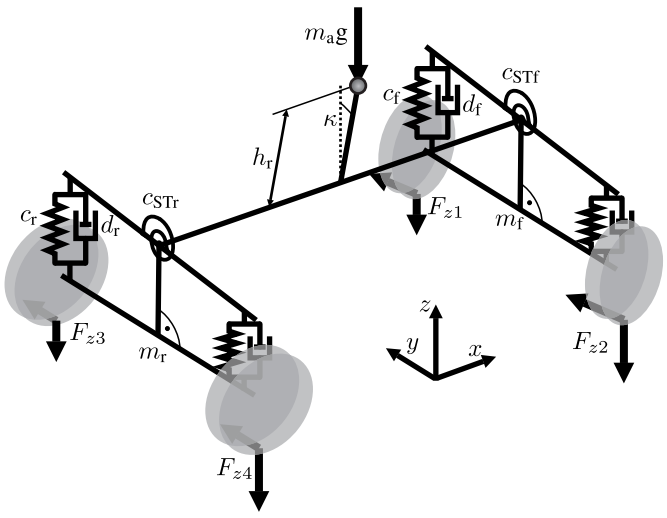

Fig. 2. Two-track model including roll dynamics of a vehicle performing a left turn. The different wheel loads F_{zi}, the spring-damper systems and the system's state κ are displayed.

equations of motion

$$\begin{aligned} J_z\ddot{\Psi} &= l_\mathrm{f}\left(F_{y1}+F_{y2}\right)\cos\left(\delta\right) - l_\mathrm{r}\left(F_{y3}+F_{y4}\right) - \sum_{i=1}^{4} M_i\,, \\ mv\left(\dot{\beta}+\dot{\Psi}\right) &= \left(F_{y1}+F_{y2}\right)\cos\left(\beta-\delta\right) + \left(F_{y3}+F_{y4}\right)\cos\beta\,, \\ m_\mathrm{a}h_\mathrm{r}a_y &= J_\kappa\ddot{\kappa} + d_\kappa\dot{\kappa} + c_\kappa\kappa - m_\mathrm{a}gh_\mathrm{r}\kappa\,, \end{aligned} \tag{1}$$

with the distance between front and rear axis to the center of gravity (cog) $l_{\mathrm{f,r}}$, respectively, mass m, moment of inertia with respect to the vertical axis J_z, velocity and lateral acceleration of the cog v, a_y, and self-aligning torques M_i. Roll dynamics are represented in analogy to a spring-damper system with gravitational influence with chassis mass m_a, distance between roll axis and cog h_r, moment of inertia with respect to the roll axis J_κ, gravitational acceleration g, and spring and damper constant c_κ and d_κ, respectively. The input of the system is the steering angle δ, which represents the angle between the vehicle's and tire's longitudinal axis. The lateral forces F_{yi} are the leading quantities in these equations depending on the tire's skew angles α_i. In general, the skew angle can be described as angle between the tire's velocity vector and its longitudinal axis, so it can be expressed as $\alpha_i = \delta - \arctan\left(\frac{v_{yi}}{v_{xi}}\right)$, which leads to

$$\begin{aligned} \alpha_{1,2} &= \delta - \arctan\left(\frac{l_\mathrm{f}\dot{\Psi} + v\sin\beta + h_\mathrm{r}\dot{\kappa}}{v\cos\beta \pm \frac{b_\mathrm{f}}{2}\dot{\Psi}}\right), \\ \alpha_{3,4} &= \quad -\arctan\left(\frac{l_\mathrm{r}\dot{\Psi} - v\sin\beta + h_\mathrm{r}\dot{\kappa}}{v\cos\beta \pm \frac{b_\mathrm{r}}{2}\dot{\Psi}}\right) \end{aligned} \tag{2}$$

for the considered two-track model including roll dynamics.

B. Tire Model

Considering the introduced model the lateral forces F_{yi} can be expressed as follows:

$$F_{yi} = \mu \cdot f(\alpha_i) \cdot g(F_{zi}), \tag{3}$$

where μ is the friction coefficient of the tire-road contact and $f(\alpha_i)$ and $g(F_{zi})$ representing point-symmetric, non-linear functions depending on the skew angles and wheel loads, respectively. The function $f(\alpha_i)$ is commonly expressed by the Magic Formula Tire Model [6]:

$$f(\alpha_i) = \sin\left(C \arctan\left(\frac{B}{\mu}\alpha_i\right) - E\left(\frac{B}{\mu}\alpha_i - \arctan\left(\frac{B}{\mu}\alpha_i\right)\right)\right), \tag{4}$$

with empirical parameters B, C and E.

The nonlinear function $g(F_{zi})$ represents the influence of wheel loads on the tire's lateral force by

$$g(F_{zi}) = \frac{F_{z0i}}{1-e^{-k}}\left(1 - e^{\left(-\frac{k}{F_{z0i}}F_{zi}\right)}\right), \tag{5}$$

with parameter k varying the relation in $g(F_{zi})$, F_{zi} being the wheel loads and F_{z0i} being the wheel loads in absence of lateral and roll acceleration [19]. Furthermore, the tire's dynamic behavior is modeled by a delay unit of first order by

$$F_{yi} + \frac{l_\mathrm{t}}{v}\dot{F}_{yi} = \mu \cdot f(\alpha_i) \cdot g(F_{zi}), \tag{6}$$

with a time constant proportional to a tire-delay constant l_t and anti-proportional to the vehicle's velocity v. All the parameters introduced in (1)-(5) are identified using a particle swarm algorithm [20] comparing simulation results to measurements taken with a real vehicle during different driving maneuvers [19].

III. Kalman Filtering

The Kalman Filter is an algorithm for state estimation of linear dynamic systems corrupted by stochastic noise, including an underlying parametric model of the system and a series of (noisy) measurements [8]. Its iterative nature allows for online estimation, separated in two consecutive steps, the process and the measurement update. Depending on the uncertainties of model and measurement, respectively, a Kalman gain K_k is calculated at every time step which weights the influence of the model and the measurement on the current state estimate. Therefore, the model of the physical system (1) need to be available in discretized form, for example using Taylor-Lie series expansion [21]. In general a linear, discrete system corrupted by additive noise can be described as

$$\begin{aligned} x_k &= Ax_{k-1} + Bu_{k-1} + w_{k-1} \\ y_k &= Hx_k + v_k, \end{aligned} \tag{7}$$

with x_k being the system's state vector at the discrete time k, u_k being the system's input vector, and y_k being the measurement vector. The random variables w and v represent the process and measurement noise, respectively. They are assumed to be independent of each other with normal probability distributions $p(w) \propto \mathcal{N}(0,Q)$ and $p(v) \propto \mathcal{N}(0,R)$, with Q and R being the process and measurement covariance matrices, respectively.

Since the introduced model in Sec. II describes the system according $x_k = f(x_{k-1}, u_{k-1}, w_{k-1})$ and $y_k = h(x_k, u_k, v_k)$ the model is highly non-linear. Therefore, the linear Kalman Filter is not able to estimate the side-slip angle with high quality. Consequently, generalized algorithms called Extended Kalman Filter (EKF) or Unscented Kalman Filter (UKF), using different approaches in estimating non-linear dynamic systems, need to be implemented. Their origin and mathematical implementation will be introduced in the following.

A. Extended Kalman Filter

The EKF uses nearly the same equations as the Kalman Filter, except that process and measurement models as well as the noise representation of the non-linear system are linearized. Assuming the initial state representation to be a normal distributed random variable with mean $\bar{x}$ and covariance P_x, the estimated distribution will be normally distributed at every time step, due to the linearized system equations. Therefore, the estimated state can easily be assumed to be the expectation value of this distribution. The noise, corrupting the system and measurement model will again be represented by additive stochastic terms $p(w) \propto \mathcal{N}(0,Q)$ and $p(v) \propto \mathcal{N}(0,R)$. The following equations describe the iterative work flow of the EKF in two steps:

1) Process Update:

$$\begin{aligned} x_k^\dagger &= f(x_{k-1}, u_{k-1}, 0), \\ P_k^\dagger &= A_k P_{k-1} A_k^T + W_k Q_{k-1} W_k^T. \end{aligned} \tag{8}$$

2) Measurement Update:

$$\begin{aligned} K_k &= P_k^\dagger H_k^\dagger \left(H_k P_k^\dagger H_k^T + V_k R_k V_k^T\right)^{-1}, \\ \hat{x}_k &= x_k^\dagger + K_k\left(y_k - h\left(x_k^\dagger, 0\right)\right), \\ \hat{P}_k &= (1 - K_k H_k) P_k^\dagger. \end{aligned} \tag{9}$$

In these equations $x_k^\dagger$ and $P_k^\dagger$ represent the state and covariance after the process update. It is notable, that no noise is considered during the process update of the system's state x_k. The calculated quantities $x_k^\dagger$ and $P_k^\dagger$ are used during the measurement update to calculate new state and covariance estimates $\hat{x}_k$ and $\hat{P}_k$. The Matrices A and H represents the Jacobian Matrix of partial derivatives of the system and measurement model, respectively, with respect to the system's state. W and V describe the linearized model and measurement noise representations.

B. Unscented Kalman Filter

The Unscented Kalman Filter uses a different approach in estimating a random state variable x with mean $\bar{x}$ and covariance P_x. For this purpose, the state random variable is redefined as a concatenation of the initial state and noise variables [12]. Therefore, no restriction to the assumed

noise representation has to be made. Using the unscented transformation [22], a set of carefully chosen sigma-points

$$\begin{aligned} x_0 &= \bar{x} \\ x_i &= \bar{x} + \left(\sqrt{(L+\lambda)P_x}\right)_i, \qquad i = 1,...,L \\ x_i &= \bar{x} - \left(\sqrt{(L+\lambda)P_x}\right)_{i-L}, \qquad i = L+1,...,2L \end{aligned} \tag{10}$$

is transformed through the non-linear function $x_k = f(x_{k-1}, u_{k-1}, w_{k-1})$ (1) (Fig. 3), capturing up to the third order moment of the random variable for any non-linearity, where λ is a scaling parameter, L is the dimension of the augmented state vector x and $\left(\sqrt{(L+\lambda)P_x}\right)_i$ is the ith row of the matrix square root, e.g. using the Cholesky decomposition. Using these sigma points, the estimation process can again be expressed in two steps:

1) Process update:

$$\begin{aligned} x_{k,i} &= f(x_{k-1,i}, u_{k-1}, w_{k-1}), \\ x_k^\dagger &= \sum_{i=0}^{2L} W_i^m x_{k,i}, \\ P_k^\dagger &= \sum_{i=0}^{2L} W_i^c \left(x_{k,i} - x_k^\dagger\right)\left(x_{k,i} - x_k^\dagger\right)^T. \end{aligned} \tag{11}$$

2) Measurement update:

$$\begin{aligned} y_{k,i} &= h(x_{k,i}, u_k, v_k), \\ y_k^\dagger &= \sum_{i=0}^{2L} W_i^m y_{k,i}, \\ K_k &= P_{xy} \cdot P_{yy}^{-1}, \\ \hat{x}_k &= x_k^\dagger + K_k\left(y_k - y_k^\dagger\right), \\ \hat{P}_k &= P_k^\dagger - K_k P_{yy} k_k^T. \end{aligned} \tag{12}$$

$W^{m,c}$ represent weighting factors depending on the initial parameters of the UKF. It is notable, that the sigma points undergo the real noise corrupted non-linear transformation $x_k = f(x_{k-1}, u_{k-1}, w_{k-1})$ and the covariance is calculated for the transformed sigma points at every time step. This approach does not need any linearization and, therefore, even states of systems that are not continuous or not continuously differentiable can be estimated using this algorithm.

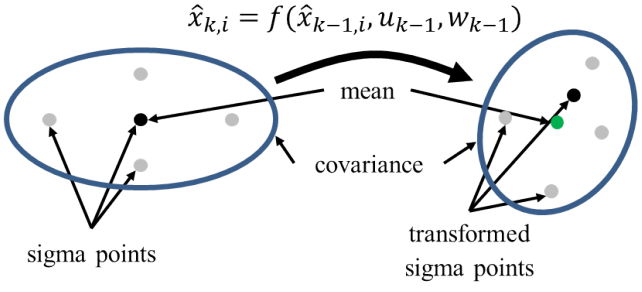

Fig. 3. Schematic representation of the Unscented Transformation in two dimensions. The five sigma points (gray and balck dots) undergo the nonlinear transformation $x_k = f(x_{k-1}, u_{k-1}, w_{k-1})$, followed by a calculation of the new mean (green dot) and covariance by means of weighted sums.

In summary both approaches use different ways to estimate a random state variable. The EKF uses linearization of the underlying equations and, therefore, calculates the Gaussian distributions analytically for every time step. The UKF approximates the random variable's distribution with sigma-points and calculates new mean and covariance using these sigma points for every time step. Consequently, no linearizations have to be made. Furthermore, an augmented state variable including all noise representations is used, able to represent any source of noise.

IV. Estimation Results

For the validation of the introduced methodologies the estimation of the vehicles side-slip angle is presented using both, the EKF and UKF and compared to measurements of a real vehicle's side-slip angle during these maneuvers taken by a Correvit sensor added to the vehicle. The measurements used within the Kalman Filter algorithms are taken from the vehicle's CAN-Bus with a sample frequency of 200 Hz, so that no additional sensors need to be implemented and online implementation of the algorithm can be simulated. In this realization the yaw-rate and the lateral acceleration measurements are used during the Kalman Filter algorithm and, furthermore, the measured steering angle and velocity are used as inputs. This leads to the augmented state, measurement and input vectors

$$\begin{aligned} x &= [\dot{\Psi}, \beta, \kappa, \dot{\kappa}, F_1, F_2, F_3, F_4, w, v]^T, \\ y &= [\dot{\Psi}, a_y]^T, \\ u &= [\delta, v]^T. \end{aligned} \tag{13}$$

Two different driving scenarios on dry surfaces are introduced. First, a highly dynamic double-lane change, simulating an evasive maneuver. Second, a step steering input, where the vehicle drives with a constant velocity and an abrupt steering input is performed. For both maneuvers the settings of each Kalman Filter stays the same, so that an optimal compromise that satisfies for both maneuvers has to be found. In summary the normalized mean square error (NMSE) for all maneuvers can be found in tabular I. In Fig. 4 a double-lane change maneuver with a velocity of around 27.0 m/s (97.2 km/h) and lateral acceleration up to 8 m/s^2 is presented. The estimation results for the EKF (red line) and the UKF (blue line) show almost the same behavior for both estimators and achieve good performance on estimating the vehicle's sides-slip (NMSE: EKF: 0.8879, UKF: 0.8899) (upper part of Fig. 4). Even during parts with high lateral accelerations and large side-slip angles a good performance is achieved. Slight differences of both estimators can be seen during these parts, e.g. between four and five seconds and after seven seconds, where the UKF's estimation reaches a better compliance. The lower part of Fig. 4 shows the yaw-rate and lateral acceleration during this maneuver. It can be seen, that the estimators again reach good compliance for both estimators.

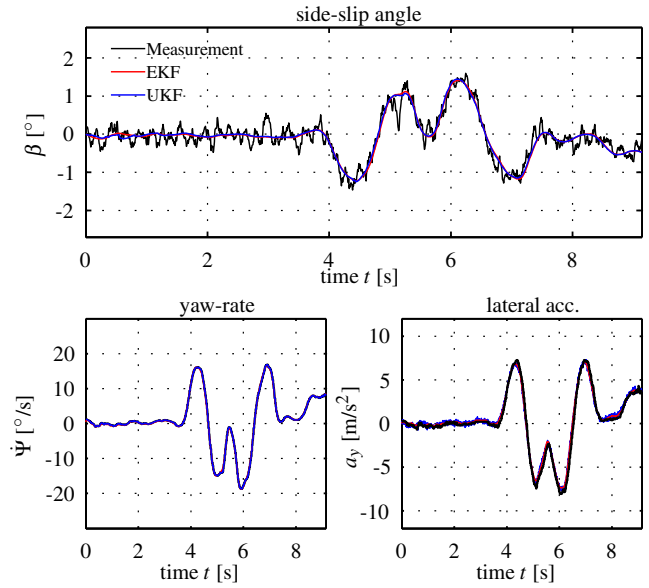

Fig. 4. Measured and estimated side-slip angle, yaw-rate and lateral acceleration during a double-lane change maneuver with a speed of 27.0 m/s (97.2 km/h). Lateral accelerations up to 8 m/s^2 are reached.

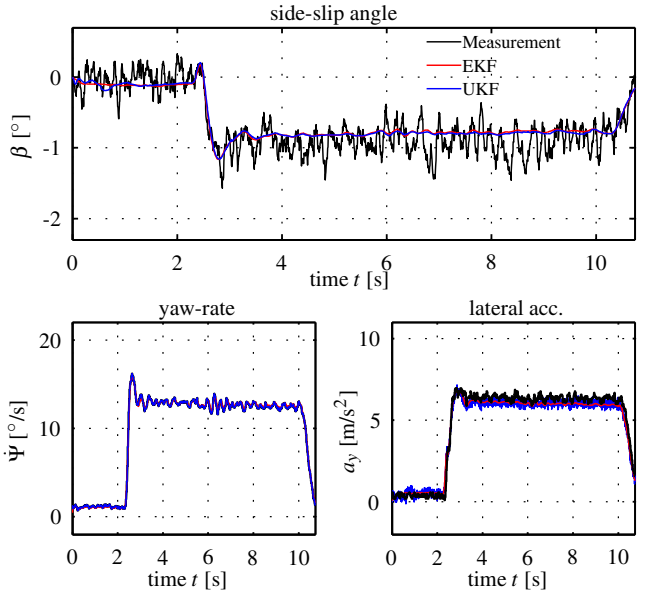

Fig. 6. Estimation results for side-slip, yaw-rate and lateral acceleration during a steering step maneuver with a velocity of 27.2 m/s (97.9 km/h) and lateral accelerations of almost 7 m/s^2 are presented.

In Fig. 5 a more dynamic double lane-change maneuver with a velocity of around 25.7 m/s (92.5 km/h) and lateral acceleration over 9 m/s^2 is presented. Again, both estimators show a good compliance between estimated side-slip angle and reference measurement, except between six and seven seconds, where the EKF's compliance is better (NMSE: EKF: 0.9182, UKF: 0.9194). Furthermore, the estimation of yaw-rate and lateral acceleration shows good performance. Considering the lateral acceleration a difference of estimation and reference measurement can be seen between four and six seconds for both estimators.

In Fig. 6 a steering step maneuver with a constant velocity of 27.2 m/s (97.9 km/h) and lateral accelerations of almost 7 m/s^2 is shown. Again, both estimators show good performances for the side-slip estimation, especially during the step (NMSE: EKF: 0.7582, UKF: 0.7661). A slightly better performance of the UKF can be seen after the step, since the estimation is little smoother and closer to the reference

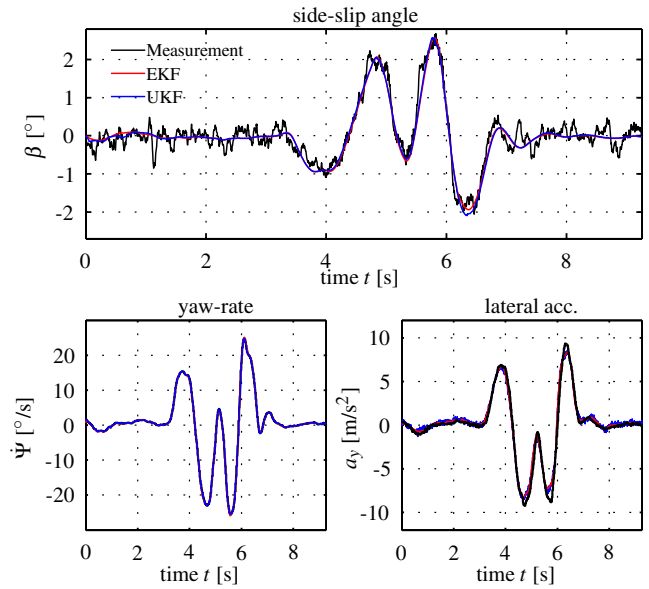

Fig. 5. Measured and estimated side-slip angle, yaw-rate and lateral acceleration during a second, more dynamic double-lane change maneuver with a speed of 25.7 m/s (92.5 km/h) with EKF and UKF are shown. Lateral accelerations above 9 m/s^2 are reached.

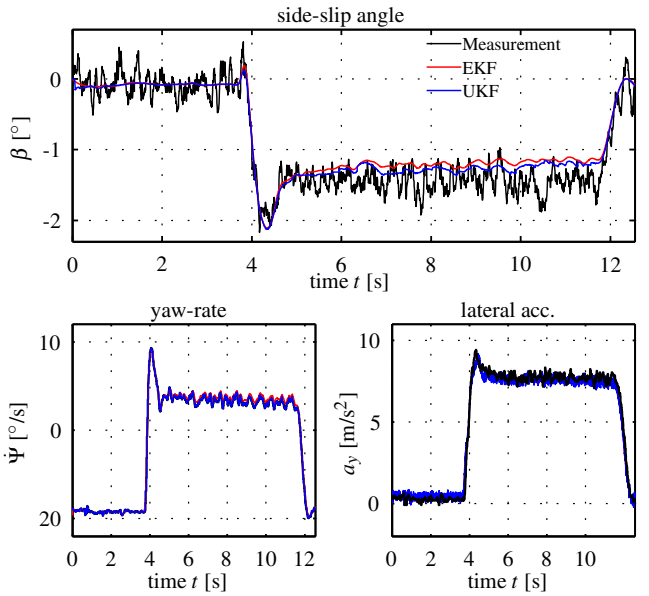

Fig. 7. Estimation results for side-slip, yaw-rate and lateral acceleration during a steering step maneuver with a velocity of 31.5 m/s (113.4 km/h) and lateral accelerations of above 9 m/s^2 are presented.

TABLE I

This table shows the normalized mean square error (NMSE) of side-slip estimation using EKF and UKF for all four presented maneuvers.

NMSE	Double Lane Change		Steering Step	
	1	2	1	2
EKF	0.8879	0.9182	0.7582	0.8734
UKF	0.8899	0.9194	0.7661	0.9040

measurement. Considering yaw-rate and lateral acceleration estimation a good compliance is notable, observing a severe noise of the UKF's estimation.

A second steering step maneuver is presented in Fig. 7 with a higher velocity of $31.5\,\mathrm{m/s}$ ($113.4\,\mathrm{km/h}$) and lateral accelerations of above $9\,\mathrm{m/s^2}$. Again, both estimators show good compliance of estimated side-slip angle and reference measurement during the step, but afterwards the UKF shows better performance (NMSE: EKF: 0.8734, UKF: 0.9040). Furthermore, a difference for yaw-rate estimation is notable. At the steering step, both estimators show almost the same behavior, but afterwards the UKF's estimation shows better compliance. For the lateral acceleration the UKF shows very good performance, even reproducing the measurement's noise very good.

Summing up, both estimators show good performance in estimating the vehicle's side-slip angle for both maneuvers, with a slightly better performance of the UKF. For higher velocities the UKF overcomes the EKF's performance. Thus, it can be demonstrated, that the UKF achieves higher accuracy for different maneuvers without changing the initial settings.

V. CONCLUSIONS AND OUTLOOK

In this paper a highly non-linear model of vehicle's lateral dynamics with three degrees of freedom is presented. Furthermore, the Extended and Unscented Kalman Filter are introduced and used for state estimation of the vehicle's side-slip angle with an enlarged number of states. Comparison of the estimated state and measurements taken on a real vehicle for two different maneuvers show good compliance for both estimators. Overall, the UKF seems to overcome the EKF's performance, especially considering one setting of the initial filter for both maneuvers.

The next step in improving the estimation's accuracy is to build up a more detailed model of vehicle's dynamics considering longitudinal and vertical dynamics. Furthermore, more driving maneuvers with different velocities and higher lateral accelerations need to be analyzed. Considering varying environmental influences an accurate state estimation on different surfaces, e.g. ice, snow, needs to be guaranteed. Therefore, a parameter estimation of friction coefficient between tires and road has to be implemented. In this context, a sensitivity based dual or joint estimation of the vehicle's side-slip angle and the friction coefficient needs to be realized and verified using additional maneuvers on different surfaces.

ACKNOWLEDGMENT

We would like to thank the Institute of Automotive Engineering (IfF) form Technische Universität Braunschweig, Germany for providing the VW Golf GTI measurement data.

REFERENCES

[1] D.M. Bevly, J.C. Gerdes, C. Wilson, and Gengsheng Zhang. The use of GPS based velocity measurements for improved vehicle state estimation. In *American Control Conference, 2000. Proceedings of the 2000*, volume 4, pages 2538–2542 vol.4, 2000.

[2] R. Anderson and D.M. Bevly. Estimation of slip angles using a model based estimator and GPS. In *American Control Conference, 2004. Proceedings of the 2004*, volume 3, pages 2122–2127 vol.3, June 2004.

[3] M.C. Best, T.J. Gordon, and P.J. Dixon. An extended adaptive kalman filter for real-time state estimation of vehicle handling dynamics. *Vehicle System Dynamics*, 34(1):57–75, 2000.

[4] F. Cheli, E. Sabbioni, M. Pesce, and S. Melzi. A methodology for vehicle sideslip angle identification: comparison with experimental data. *Vehicle System Dynamics*, 45(6):549–563, 2007.

[5] M. Doumiati, A.C. Victorino, A. Charara, and D. Lechner. Onboard real-time estimation of vehicle lateral tire-road forces and sideslip angle. *IEEE/ASME Transactions on Mechatronics*, 16(4):601–614, August 2011.

[6] E. Bakker, L. Nyborg, and H. B. Pacejka. Tyre modelling for use in vehicle dynamics studies. Technical report, Chassis Engineering, Volvo Car Corp., 1987.

[7] B. Bossdorf-Zimmer. *Nichtlineare Fahrzustandsbeobachtung für die Echtzeitanwendung*. PhD thesis, TU Braunschweig, 2007.

[8] G. Welch and G. Bishop. *An Introduction to the Kalman Filter*. 1995.

[9] T. A. Wenzel, K. J. Burnham, M. V. Blundell, and R. A. Williams. Dual extended kalman filter for vehicle state and parameter estimation. *Vehicle System Dynamics*, 44(2):153–171, 2006.

[10] B.-C. Chen and F.-C. Hsieh. Sideslip angle estimation using extended kalman filter. *Vehicle System Dynamics*, 46(sup1):353–364, 2008.

[11] J. Dakhlallah, S. Glaser, S. Mammar, and Y. Sebsadji. Tire-road forces estimation using extended kalman filter and sideslip angle evaluation. In *American Control Conference, 2008*, pages 4597–4602, June 2008.

[12] E.A. Wan and R. Van der Merwe. The unscented kalman filter for nonlinear estimation. In *Adaptive Systems for Signal Processing, Communications, and Control Symposium 2000. AS-SPCC. The IEEE 2000*, pages 153–158, 2000.

[13] Junquan Li, M.A Post, and R. Lee. A novel adaptive unscented kalman filter attitude estimation and control systems for 3u nanosatellite. *Control Conference*, 2013.

[14] H. Zhang, H. Yan, F. Yang, and Q. Chen. Distributed average filtering for sensor networks with sensor saturation. *IET Control Theory Applications*, 2013.

[15] R. Konrad. Using the unscented kalman filter and a non-linear two-track model for vehicle state estimation. *IFAC World Congress*, pages 8570–8575, July 2008.

[16] S. Antonov, A. Fehn, and A. Kugi. Unscented kalman filter for vehicle state estimation. *Vehicle System Dynamics*, 49(9):1497–1520, September 2011.

[17] H. Abdellatif, B. Heimann, and J. Hoffmann. Nonlinear identification of vehicle's coupled lateral and roll dynamics. *Proc. of the 11th IEEE Mediterranean Conference on Control and Automation*, 2003.

[18] Houssem Abdellatif. Accurate modelling and identification of vehicle's nonlinear lateral dynamics. In Pavel Zítek, editor, *Proceedings of the 16th IFAC World Congress*, pages 1241–1241, July 2005.

[19] M. Wielitzka, M. Dagen, and T. Ortmaier. Nonlinear modeling and parameter identification of vehicle's lateral dynamics. *Advanced Vehicle Control*, 2014.

[20] I. C. Trelea. The particle swarm optimization algorithm: convergence analysis and parameter selection. *Information Processing Letters*, 85(6):317 – 325, 2003.

[21] S. Hohmann. Stabilitätseigenschaften nichtlinearer abtastsysteme (stability properties of nonlinear sampled-data systems). *at – Automatisierungstechnik/Methoden und Anwendungen der Steuerungs-, Regelungs- und Informationstechnik*, 51(12/2003):563–573, December 2003.

[22] S.J. Julier. The scaled unscented transformation. In *American Control Conference, 2002. Proceedings of the 2002*, volume 6, pages 4555–4559 vol.6, 2002.